Synthesis, transacylation kinetics and computational chemistry of a set of arylacetic acid 1β-*O*-acyl glucuronides†‡

Neil G. Berry,[a] Lisa Iddon,[a] Mazhar Iqbal,§[a] Xiaoli Meng,[a] Prabha Jayapal,¶[a] Caroline H. Johnson,[b] Jeremy K. Nicholson,[b] John C. Lindon,[b] John R. Harding,[c] Ian D. Wilson[c] and Andrew V. Stachulski*[a]

Received 18th December 2008, Accepted 20th March 2009
First published as an Advance Article on the web 27th April 2009
DOI: 10.1039/b822777b

Many widely-used non-steroidal anti-inflammatory agents (NSAIDs), e.g. ibuprofen, are extensively metabolised as their acyl glucuronides (AGs), and the reactivity of these AGs raises important questions regarding drug safety and toxicity. In order to understand better the structure–reactivity of these metabolites, we have performed a detailed study of the synthesis, structural analysis and computed transacylation reactivity of a set of acyl glucuronides (AGs) of phenylacetic acids with varying α-substitution. A selective acylation procedure was used to prepare all the desired 1-(phenyl)acetyl-β-D-glucopyranuronic acids **9**, **12**, **13** and **15** as single 1β-anomers in good yields. Their reactivity was measured using ^{1}H NMR spectroscopy in pH 7.4 buffer: the dominance of transacylation over hydrolysis in this system was confirmed together with the measurement of half-lives of the 1β-isomers of the AGs. The half-lives ranged from 20 min for compound **9** to 23 h for **15**. The lack of any significant concentration dependence of the reactivity suggests that the main mechanism is intramolecular. A novel computational chemistry and modelling study was performed on both the ground states of the AGs and the transition states for acyl migration to search for correlations with the kinetic data and to probe the mechanistic detail of the acyl transfer. An excellent degree of correlation was found between the calculated activation energies and the rates of transacylation. Especially, transition state analysis provided for the first time a firm mechanistic explanation for the slower kinetics of the (*S*)-isomer AG **13** compared to the (*R*)-isomer **12**, thus throwing important light on the pharmacokinetic behaviour of marketed NSAIDs.

Introduction

Non-steroidal anti-inflammatory drugs (NSAIDs) are among the most used, and prescribed, of all therapeutic classes. An estimated annual sales figure of $9.2 billion was reported for the year ending Sept. 30th 2006. Ibuprofen, naproxen and diclofenac especially, all in the subdivision of arylacetate or arylpropionate NSAIDs, are very widely used to treat both acute and chronic inflammatory conditions. There have been a number of problems associated with NSAIDs in terms of adverse effects, ranging from direct toxicity in the liver or kidney to hypersensitivity effects, and several have been withdrawn from the market for this reason.

A characteristic of the above compounds is that they are all carboxylic acids and hence extensively metabolised *in vivo* as their acyl glucuronides (AGs), initially as single 1β-anomers, following enzyme-mediated reaction with uridine diphosphate-glucuronic acid (UDPGA) in the body. AGs constitute an important class of *O*-glucuronides which are vital conjugates in phase 2 metabolism, generally acting in a detoxifying mode[1,2] Such AGs were first reported by Goebel in 1938.[3] It was gradually appreciated[4–6] that AGs were considerably more reactive than *O*-alkyl or *O*-aryl glucuronides, both in their chemical behaviour and in their ability to interact with body proteins. In a recent review[7] we have highlighted advances in the synthesis, analysis and study of the biological reactivity of these important metabolites.

The empirical reactivity patterns exhibited by AGs are now well understood, and are shown in Fig. 1. Two principal pathways operate: either direct reaction of nucleophiles at the ester carbonyl group may liberate the aglycone directly (Pathway 1), or a base-catalysed migration of the ester may result, leading to a complex mixture of positional acyl isomers and anomers (Pathway 2). This migratory behaviour is significant at physiological pH, whereas AGs are invariably more stable in the pH range 3–5 as previously

[a]*Robert Robinson Laboratories, Department of Chemistry, University of Liverpool, Liverpool, UK L69 7ZD. E-mail: stachuls@liv.ac.uk; Fax: +44(0)151 794 3588; Tel: +44(0)151 794 3542*
[b]*Department of Biomolecular Medicine, Division of Surgery, Oncology, Reproductive Biology and Anaesthetics (SORA), Faculty of Medicine, Sir Alexander Fleming Building, Imperial College London, South Kensington, London, UK SW7 2AZ*
[c]*DMPK, AstraZeneca Pharmaceuticals, Mereside, Alderley Park, Macclesfield, Cheshire, UK SK10 4TG*

† While this work was being written up, another study of acyl glucuronide reactivity was published, though without any computational chemistry (A. Baba and H. Yoshioka, *Chem. Res. Toxicol.*, 2009, **22**, 158–172). We note that the authors also made use of the ^{13}C carbonyl C chemical shift as a marker for reactivity which we refer to.

‡ Electronic supplementary information (ESI) available: Synthesis of compound **7**; photocopies of NMR spectra for compounds **10**, **11** and **14**; detailed NMR procedures for the kinetic studies and ^{13}C spectra; computational data of parameters used in the DFT study are appended, as well as figures and detailed coordinates of transition states. See DOI: 10.1039/b822777b

§ Present address: National Institute for Biotechnology and Genetic Engineering, NIBGE, Jhang Road, Faisalabad, Pakistan.

¶ Present address: Lehrstuhl für Theoretische Chemie, Universität Bonn, Wegelerstraße 12, D-53115 Bonn, Germany.

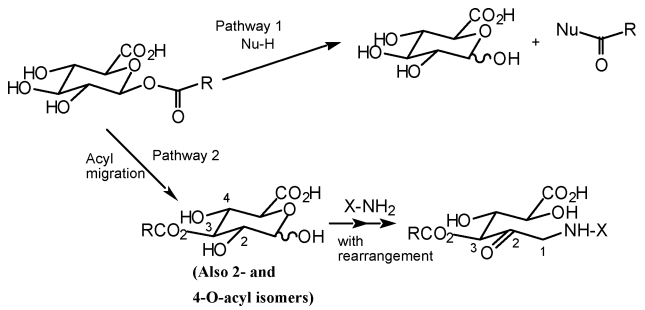

Fig. 1 Chemical reactivity of acyl glucuronides.

noted.[8,9] Following migration, direct reaction with amines, *e.g.* those of protein side-chains, may occur yielding initially imines, then rearranged amines as shown, by the so-called Amadori rearrangement.[6,10,11]

A number of studies have investigated AG reactivity using both MS and NMR spectroscopy.[12–23] To obtain detailed kinetic information, most studies have been performed *in vitro* using buffer at pH 7.4. In this case, transacylation dominates over hydrolysis whilst *in vivo* hydrolysis might be more important.[24] To investigate the stability of the 1β-isomer alone, it is sufficient to allow the reaction to proceed spontaneously. Here the simple loss of the 1β-isomer can be seen to be approximately first-order in nature and hence the rate of degradation (k_d) is a good surrogate for transacylation kinetics. To deduce the kinetic parameters for other isomerization reactions shown in Fig. 1, it has proved necessary to separate the reacting species in a directly-coupled HPLC–NMR experiment and to hold each isomer in the NMR probe while its isomerisation reactions proceed.[20,25,26]

In the case of AGs of benzoic acids, the half-lives and degradation rates may be predicted successfully by a Hammett-type correlation.[14,27] For arylacetic acids, the kinetics are more complex, with both electronic and steric factors being involved.[10,11,19,28] Since this class includes the AGs of frequently-used drugs such as diclofenac, ibuprofen and clofibrate, it is important to measure accurately their degradation kinetics[22] and ideally be able to predict the reactivity of new drugs of related structure.

A range of experimental approaches for measuring the transacylation kinetics of AGs in solution has been developed[20,29–31] and, *inter alia*, we have recently conducted an NMR study on the transacylation behaviour of synthetic ibuprofen AG, its major human metabolites, and its esters.[18]

Now we present a detailed study of the chemical synthesis and reactivity, as measured by ^{1}H NMR spectroscopy, of the AGs of phenylacetic acid and its mono- and di-α-methylated analogues. These compounds may be considered as models for the arylacetic acid class of NSAIDs and allow us to probe, in particular, the effect of α-substitution, and hence an important steric constraint, on reactivity. Additionally we present a molecular modelling study in which we have calculated ground and transition state structures and activation energies to attempt to discern the factors that govern transacylation rates. This allowed us to confirm previous empirical observations of the relative migration rates of (*R*)- and (*S*)-AG diastereoisomers.

Results

Synthesis

It was essential in the first place to synthesise the required AGs as single 1β-anomers. We have previously shown that this can be achieved[32,33] in high yield and excellent β-selectivity through the selective acylation of either allyl or benzyl D-glucuronate **1** and **2**, Fig. 2, employing *O*-(7-azabenzotriazolyl-1-yl)-N,N′- tetramethyluronium hexafluorophosphate (HATU)–NMM followed by appropriate deprotection. We demonstrate here a new and useful variant of this method, namely the application of 4-methoxybenzyl (PMB) D-glucuronate **3** which was prepared similarly to **1** and **2**, in very good yield, by base-catalysed alkylation of D-glucuronic acid **4** with 4-methoxybenzyl bromide. As in our earlier work,[32] a polymer-bound fluoride was a convenient base, or tetra-*n*-butylammonium fluoride (TBAF) could be used.

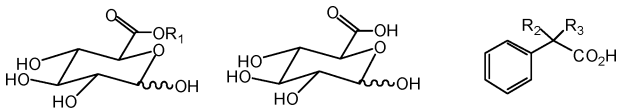

1 $R_1 = CH_2CH{=}CH_2$ **4** **5** $R_2 = R_3 = H$

2 $R_1 = PhCH_2$ **6** R_2 =Me, $R_3 = H$

3 $R_1 = 4\text{-}MeOC_6H_4CH_2$ **7** $R_2 = R_3 = Me$

Fig. 2 Carbohydrate intermediates and carboxylic acids used in this study.

The selective acylation method was then applied to carboxylic acids **5**, **(±)-6** and **7**. Following selective acylation[32] of **3** with **5** using HATU–NMM, deprotection of the resulting PMB ester **8** (Fig. 3) was conveniently achieved[34,35,36] by brief treatment with 10% TFA in dichloromethane, avoiding metal catalysts altogether. This method exploits the greater stability of AGs in acid solution noted above[8,9,37] and no significant cleavage of the ester link was observed: **9** was obtained in excellent purity. The presence of traces of water assisted this deprotection; in our example it was not necessary to add anisole as a cation scavenger[34,36] but this will depend on the exact aglycone structure.

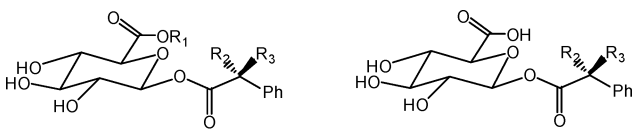

8 $R_1 = 4\text{-}MeOC_6H_4CH_2$, $R_2 = R_3 = H$ **9** $R_2 = R_3 = H$

10 $R_1 = PhCH_2$, $R_2 = Me$, $R_3 = H$ **12** $R_2 = Me$, $R_3 = H$

11 $R_1 = PhCH_2$, $R_2 = H$, $R_3 = Me$ **13** $R_2 = H$, $R_3 = Me$

14 $R_1 = PhCH_2$, $R_2 = R_3 = Me$ **15** $R_2 = R_3 = Me$

Fig. 3 Acyl glucuronides prepared and their glucuronate ester precursors.

Following coupling of **(±)-6** with **2**, the diasteroisomeric esters **10** and **11** were readily separated by chromatography and cleanly deprotected by catalytic hydrogenation as described,[33] yielding acids **12** and **13**. The absolute stereochemistry of the (*R*)-isomer AG was confirmed by hydrolysis of the AG **12** and comparison by HPLC with a sample of authentic material. α,α-Dimethylphenylacetic acid **7** is now commercially available, or it may be prepared by alkylation of α-methylphenylacetaldehyde, followed by oxidation

Table 1 First-order degradation rate constants and half-lives for the 1-β-*O*-acyl glucuronides of phenylacetic acid and its analogues, **9**, **12**, **13** and **15**

1-β-*O*-acyl glucuronide	k_d/h^{-1}	S.E[a]	$t_{1/2}$/h
R = H, H **9**	2.353	0.0010	0.29
R = H, Me (*R*) **12**	0.903	0.0004	0.78
R = H, Me (*S*) **13**	0.405	0.0002	1.71
R = Me, Me **15**	0.029	0.0001	23.30

[a] S.E = standard error for the standard least squares linear fit to the slope.

with $NaClO_2$.[38,39] Coupling of this acid was predictably slow but ester **14** was obtained in good yield and high purity; hydrogenation again afforded product **15** without difficulty.

Reactivity studies

The degradation reactions of the AGs of phenylacetic acid and its mono- and di-α-methylated analogues were investigated as described in the Experimental Section [see also ESI‡] using 600 MHz ^{1}H NMR spectroscopy in pH 7.4 buffer. The anomeric proton peak of the 1β-isomer of each AG was used to measure the degradation rate by following the decrease in intensity over the time course of the experiment. Based on the assumption of first-order kinetics, the degradation rate constants and corresponding half-lives were calculated by measuring the peak integrals, and are displayed in Table 1. Phenylacetic acid AG **9** had the fastest k_d of 2.353 h^{-1}, methylation at the α-carbon slowed the degradation to 0.903 h^{-1} and 0.405 h^{-1} for the (*R*)-**12** and (*S*)-**13** mono-α-methyl phenylacetic acid AGs respectively and 0.029 h^{-1} for the di-α-methyl phenylacetic acid AG **15**.

The hydrolysis rates of the AGs were measured from the integration of the α-glucuronic acid H1′ doublet (chemical shift ~δ 5.25) or the resolved aglycone peaks. The hydrolysis rate of the unmethylated phenylacetic AG **9** could not be measured, as the glucuronic acid H1′ doublet in this case was obscured by the presence of the H1′ doublet of the α-2-isomer at the same chemical shift, formed as a result of the rapid transacylation of this compound. The di-α-methyl phenylacetic acid AG **15** did not show any measurable hydrolysis during the transacylation period studied. The hydrolysis rates for the (*R*)-**12** and (*S*)-**13** monomethyl phenylacetic acid AGs were measured by integration of the aglycone methyl NMR peaks at δ 1.41, this being a larger signal than the glucuronic acid peaks and thus providing better sensitivity. The hydrolysis rates were estimated from a ratio of the concentrations of aglycone to the 2-*O*-acyl isomer (at the early time points when the formation of the 2-*O*-acyl isomers was first order). The zero-order hydrolysis rates were determined to be 0.045 mol dm^{-3} h^{-1} for both the (*R*)- and (*S*)-isomers, as displayed in Table 2. From these results, the first-order transacylation rates can be calculated as approximately 0.850 h^{-1} and 0.360 h^{-1} with ratios of hydrolysis to transacylation rates of 1:18 and 1:9 for the (*R*)- and (*S*)-isomers respectively.

The degradation rate for (*R*)-α-methyl-phenyl acetic acid AG **12** was also measured at a ten-fold lower concentration, 0.18 mM. In this case, the half life increased from *ca.* 0.8 h to 1.1 h. Given the precision with which such fast degradation rates can be determined using NMR spectroscopy, this is probably within the limits of the experimental error. To confirm this, another experiment was conducted on (*R*)-ibuprofen AG, where the half-lives at concentrations of 1.57 mM and 0.16 mM were 1.7 and 1.5 h respectively, showing no concentration dependence. This implies that intermolecular transacylation is at the most only a minor component of the mechanism.

Table 2 Hydrolysis rate constants for the 1-β-*O*-AGs of (*R*)- and (*S*)-α-methyl-phenylacetic acids **12** and **13**

1-β-*O*-acyl glucuronide	Ratio of aglycone : 2-*O*-acyl isomer	Hydrolysis rate/ mol dm^{-3} h^{-1}	Transacylation/ h^{-1}
R = H, Me (*R*) **12**	1:18	0.045	0.858
R = H, Me (*S*) **13**	1:9	0.045	0.360

A surrogate marker for reactivity

Previously, in a series of benzoic acid AGs, we have shown that the ^{13}C NMR chemical shift of the acyl carbonyl carbon is highly correlated with the degradation rate of the AG.[27] Hence the corresponding ^{13}C NMR chemical shifts were measured for compounds **9**, **12**, **13** and **15**. The ^{13}C carbonyl shifts found from the NMR spectra of these compounds range from ~ δ_C 170 to 175, as shown in Fig. 4. There appears to be a trend between ^{13}C chemical shift and the k_d, with the data showing that increased methylation at the α-carbon of the phenylacetic acid AGs produces a downfield (higher) NMR chemical shift, concomitant with a slower k_d. However, the (*R*)- and (*S*)-monomethylphenylacetic acid AGs **12** and **13** have almost identical ^{13}C chemical shifts, showing that the steric differences responsible for the difference in degradation rate are not mirrored by a corresponding chemical shift difference. Previous studies have shown that the presence of increasingly electronegative substituents on substituted benzoic acid AGs, causes the chemical shift to move upfield concomitant with faster degradation rates.[27,40] However, the ^{13}C NMR carbonyl chemical shift differences observed there result from predominantly electronic differences in the case of benzoic acid AGs since the shifts and kinetic parameters can both be predicted using Hammett constants.

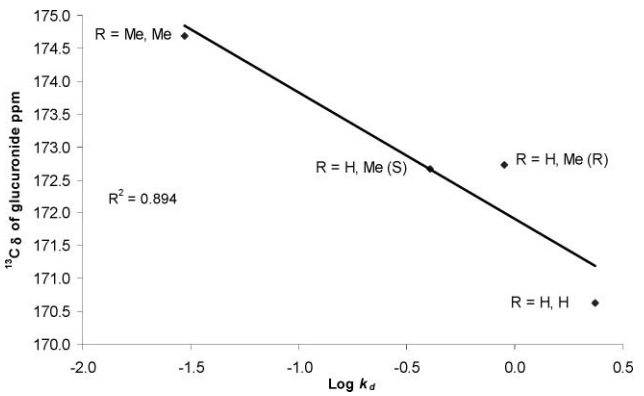

Fig. 4 ^{13}C carbonyl carbon chemical shifts of phenylacetic acid AGs **9**, **12**, **13** and **15** plotted against the logarithm of the degradation rates.

Computational chemistry

Nicholls *et al.*[31] and Pritchina *et al.*[41] have demonstrated the importance of computational calculations for providing insight into the relationships between geometrical parameters and the reaction rates of the acyl group migration. Here we have extended this approach and utilized DFT methods to determine the geometric and electronic properties of **9**, **12**, **13** and **15**, in order to search for reasons for the different kinetics seen; the acyl transfer is shown in Scheme 1.

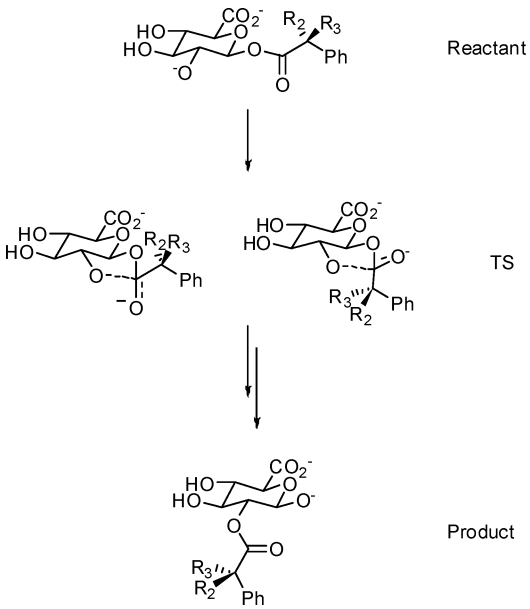

Scheme 1 Reaction studied by computational method using B3LYP/6-31G** level of theory.

A molecular mechanics conformational search of the ground state of the unmethylated AG **9** revealed seven ground state conformers with a Boltzmann distribution of 0.1 and above. Each conformer was subsequently optimised by using DFT. Five transition states were located in a similar manner, using a distance constraint (see experimental details) between the nucleophilic alkoxide oxygen and the carbonyl carbon. As the reaction proceeds to the transition state a new bond is forming between the alkoxide oxygen at the 2 position and the carbonyl carbon (distance **a**) with a concomitant elongation of the bond between the carbonyl carbon and the oxygen (distance **b**). The distance **a** becomes shorter, from 3.69–4.78Å to 1.82–2.27 Å, and the distance **b** becomes elongated, from 1.32–1.34 Å to 1.38–1.46 Å. (See ESI‡ for more details). Among the five transition states observed, TS5 (Fig. 5) follows the most favoured lowest energy pathway having activation energy 5.52 kcal/mol. The Boltzmann weighted activation energy for **9** is 5.70 kcal/mol.

In a similar fashion to **9**, six ground state conformers and five transition states have been located for **12**, the (*R*) isomer of the monomethyl AG derivative. TS5 follows the favoured lowest energy pathway with activation energy of 6.16 kcal/mol, which is higher than the activation energy for TS1 of **9**: hence **12** displays a reduced rate of transacylation. The Boltzmann weighted activation energy of **12** is 6.18 kcal/mol.

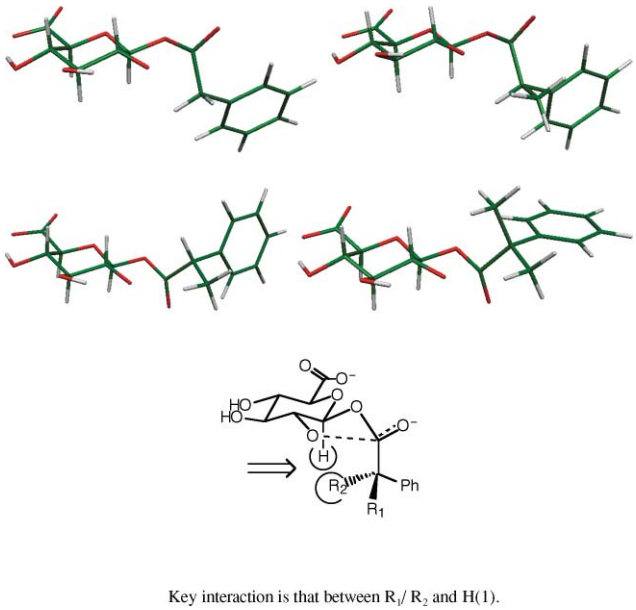

Fig. 5 Transition states of **9** (upper left, TS5), **12** (upper right, TS5) **13** (lower left, TS2) and **15** (lower right, TS1) and a schematic indicating a proposed key interaction in the TS (below).

Four transition states have been located for **13**, the (*S*) isomer of the monomethyl AG derivative. Here the lowest energy reaction path was followed by the TS2 with activation energy of 6.84 kcal/mol. The Boltzmann weighted activation energy of **13** is 6.96 kcal/mol.

Finally the activation barrier for the dimethyl AG **15** has also been calculated. Here five ground states and five transition states have been observed. The Boltzmann weighted activation energy is 9.84 kcal/mol.

Overall the calculated Boltzmann-weighted activation energies of the four molecules studied do correlate very well with the logarithm of the observed rates of transacylation measured by NMR spectroscopy, with a correlation coefficient of 0.98 (Fig. 6).

Examination of the major conformers of TS of **9** (TS5 Boltzmann Population, BP 0.76), **12** (TS5, BP 0.99), **13** (TS2, BP 0.91) and 15 (TS1, BP 0.65) reveal that the most favoured conformation for **9** and **12** has the carbonyl oxygen "up", whereas for **13** and **15** the carbonyl oxygen is "down" (Fig. 5). It is evident from the modelling that the axial hydrogen at C(1) of the pyranose ring in **9** and **12** is in close proximity to the hydrogen at the α position (2.12 Å and 2.14 Å respectively). The consequence of this is that equivalent conformations for **13** and **15** would place a considerably more bulky methyl substituent close to the axial hydrogen at C(1) of the sugar. Thus the most favoured transition states of **13** and **15** have the carbonyl oxygen "down", with the distances from the carbonyl oxygen to the axial sugar hydrogen being 2.66 Å and 2.74 Å. Examination of the data revealed that energy of solvation plays a key role in the trend in activation energies. It is proposed that the stabilisation of the transition states by solvent, presumably especially the reacting centres, is key to the reactivity. This is supported by the fact that the Boltzmann weighted ratio of the polar surface area to total surface area for these four compounds (Table 3) shows a good correlation ($r^2 = 0.84$) with the log of the transacylation rate.

Table 3 The activation barrier (Kcal/mol) for the intramolecular transacylation of AGs **9**, **12**, **13** and **15** and the partial charge on the atoms (from NPA analysis) involved in the transition states using B3LYP/6-31G**

Properties	TS1	TS2	TS3	TS4	TS5	Boltzmann Weighted
	9					
Activation energy (kcal/mol)	6.85	9.25	6.34	9.74	5.44	5.70
Partial atom charge on:						
Acyl oxygen	–0.66	–0.64	–0.63	–0.63	–0.60	–0.609
Attacking oxygen	–0.80	–0.77	–0.91	–0.86	–0.91	–0.902
Carbonyl carbon	0.83	0.83	0.84	0.84	0.84	0.839
Carbonyl oxygen	–0.76	–0.10	–0.69	–0.71	–0.69	–0.694
LUMO (Hartree)	–0.014	–0.014	–0.023	–0.016	–0.025	–0.024
Polar surface area/Total surface area	0.342	0.347	0.342	0.344	0.343	0.343
	12					
Activation energy (kcal/mol)	10.00	9.30	10.10	12.93	6.16	6.18
Partial atom charge on:						
Acyl oxygen	–0.66	–0.64	–0.65	–0.63	–0.62	–0.620
Attacking oxygen	–0.80	–0.84	–0.82	–0.88	–0.89	–0.890
Carbonyl carbon	0.84	0.84	0.84	0.85	0.84	0.840
Carbonyl oxygen	0.76	–0.74	–0.75	–0.88	–0.72	–0.718
LUMO (Hartree)	–0.013	–0.016	–0.012	–0.015	–0.019	–0.019
Polar surface area/Total surface area	0.321	0.323	0.321	0.324	0.322	0.322
	13					
Activation energy (kcal/mol)	11.13	6.84	12.54	8.22		6.96
Partial atom charge on:						
Acyl oxygen	–0.64	–0.62	–0.63	–0.65		–0.623
Attacking oxygen	–0.84	–0.92	–0.80	–0.80		–0.909
Carbonyl carbon	0.84	0.85	0.84	0.84		0.849
Carbonyl oxygen	–0.73	–0.69	–0.78	–0.77		–0.697
LUMO (Hartree)	–0.013	–0.021	–0.013	–0.013		–0.020
Polar surface area/Total surface area	0.322	0.321	0.326	0.322		0.321
	15					
Activation energy (kcal/mol)	9.54	10.15	10.53	11.82	12.86	9.84
Partial atom charge on:						
Acyl oxygen	–0.65	–0.62	–0.65	–0.64	–0.63	–0.643
Attacking oxygen	–0.8	–0.9	–0.85	–0.79	–0.86	–0.829
Carbonyl carbon	0.85	0.86	0.85	0.85	0.86	0.852
Carbonyl oxygen	–0.77	0.7	–0.72	–0.8	–0.72	–0.429
LUMO (Hartree)	–0.014	–0.013	–0.010	–0.010	–0.011	–0.013
Polar surface area/Total surface area	0.305	0.306	0.304	0.309	0.306	0.306

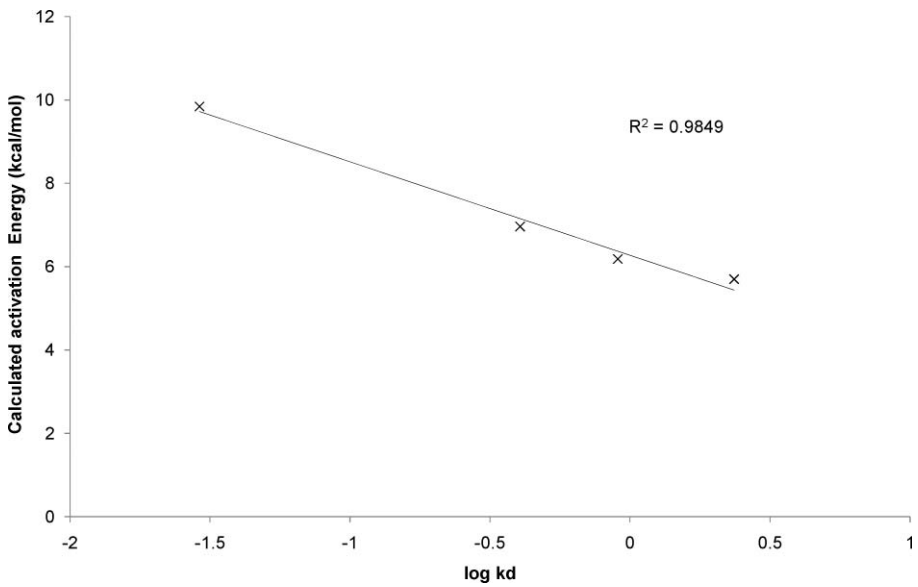

Fig. 6 Calculated Boltzmann weighted activation energy against the logarithm of degradation rates.

A number of physicochemical properties were calculated for both the ground state and transition state structures to attempt to identify a parameter that correlates with the transacylation rates (Tables S2, S3 S4, S5 in the ESI‡). For the ground states, none of these properties (Boltzmann weighted: partial atomic charges, HOMO, LUMO, normalised Fukui indices, hardness, softness, electronegativity and electrophilicity) show a good ($r^2 > 0.65$) relationship with the transacylation rate data. For the transition states there were good correlations ($r^2 > 0.75$) between transacylation rates and calculated partial atomic charges on several atoms (acyl oxygen, carbonyl carbon, carbonyl oxygen and the nucleophilic oxygen); also a good correlation ($r^2 = 0.90$) with the energy of the LUMO was observed. The other calculated parameters (HOMO, normalised Fukui indices, hardness, softness, electronegativity and electrophilicity) showed very poor correlations with the observed rates of acylation. The optimised geometries of all the ground and transition states are given in the ESI.‡

Future modelling will probe further the mechanistic pathway and calculated molecular properties alongside further data from the continuing NMR studies of a number of new synthetic analogues, with the goal of developing an *in silico* modelling protocol to predict the migratory aptitude of any given acyl group.

Discussion and Conclusions

The selective acylation method previously described by us[32,33] was applied for the efficient syntheses of the desired AGs **9**, **12**, **13** and **15** as pure 1β-isomers in good yields following deprotection. The new variant described here, using the PMB ester, will prove valuable in cases where catalytic hydrogenation or other metal-catalysed deprotection procedures are impossible owing to structural features (e.g. halogens, double bonds) in the aglycone.

The degradation of the AGs was followed by ^{1}H NMR spectroscopy, with rates calculated from the disappearance of the anomeric proton signal in the starting AG. The observed half-lives are consistent with previous observations on the AGs of arylacetic and arylpropionic acids.[7,10,11,18,19,22,28] From the measured half-lives, it is immediately clear that steric hindrance at the α-carbon is the major determining factor and that the greatest increase in half life, to 23.3 h, comes on going to the α,α-dimethyl AG **15** (Table 1). No example strictly comparable to **15** had been measured before: the case of clofibric acid ($t_{1/2}$ = 7.3 h at pH 7.4 and 37 °C)[22] shows, by comparison, a remote, rate-accelerating electronic effect by a *phenoxy* substituent whereas our *phenyl* substituent clearly has only a very small electronic effect as evinced by the ^{13}C acyl chemical shift correlation, Fig. 4. The observation of *increasing* ^{13}C chemical shifts with increasing α-methylation, but *decreasing* resulting transacylation rates, seems counter-intuitive and is not easily related to electronic factors. It may be that polar surface area, as noted in the previous section, is an outweighing factor: it decreases monotonically down the series **9**→**12**→**13**→**15** and, since it reflects solvation, is important for the transition states. Little concentration dependence of the transacylation rate was observed, indicating that *intermolecular* general base catalysis is not a significant cause of the isomerisation process, but that this is largely *intramolecular* in nature.

It is also most instructive to compare the present data with the results for (*R*)- and (*S*)-ibuprofen and other arylpropionate NSAIDs.[18,19,22] Clearly the unsubstituted phenyl ring in all our compounds, particularly **12** and **13**, leads to a significantly faster degradation rate for *both* (*R*)- and (*S*)-diastereoisomers compared to (*R*)- and (*S*)-ibuprofen (4-isobutyl group), where the half-lives are 1.8 h and 3.7 h for the (*R*) and (*S*) AGs respectively.[7] Nevertheless, the (*R*): (*S*) rate *ratio* is consistently about 2:1 for all pairs of this class. Again, using the ^{13}C acyl chemical shift correlation, the significantly slower rate for both ibuprofen isomers compared to **12** and **13** cannot be attributed to an electronic effect.

Regarding the computational study, the observed high correlation (Fig. 5), especially with the (*R*):(*S*) difference correctly predicted, is a pleasing outcome in a series where, as noted above, a complex mixture of electronic, steric and possibly other features are operating. The calculations performed are labour intensive, therefore we confined this study to the α-substitution patterns actually occurring in marketed NSAIDs. It would undoubtedly be of interest to study in the future the effect of other substitution patterns on acyl migration rate, but we feel that proof of principle has been achieved.

Since the 'profen' class of marketed NSAIDs such as ibuprofen, naproxen and ketoprofen are all of the arylpropionate (viz. mono-α-Me) series, the *R*/*S* difference is especially significant and, as we note above, is due to the existence of two distinct sets of transition states. In summary, we conclude that the (*R*)-diastereomer **12** undergoes acyl migration *via* the lower energy transition state, as adopted by the unmethylated analogue **9**, whereas the (*S*)-diastereomer **13** is forced into the higher energy transition state as adopted by the dimethyl analogue **15**. As we note above, a key interaction between the anomeric proton of the sugar ring and the α-substituent, whether H or Me, is responsible for this behaviour (further information is given in the ESI‡). This is a novel computational study and affords for the first time a mechanistic explanation of this important rate difference, which is a major factor in the different pharmacokinetics of (*R*)- and (*S*)-profens.

Our calculations assume first-order kinetics, as do the measured NMR rates (v. s.). A contribution by intermolecular general base catalysis (GBC) from one carboxylate to an adjacent molecule seemed possible *a priori*, but such GBC would require a concentration dependence of the acyl migration rate, which moreover might be different for each AG studied. However, as noted above, the lack of significant concentration dependence of the observed migration rates strongly implies that this is not a major contributor. We note that our earlier studies[18] demonstrated that esterification of the glucuronic acid moiety (removing any possibility of general base catalysis by carboxylate) led to a significant *decrease* in acyl migration rate. Further studies aimed at producing a more robust predictive model for AG half-lives and migratory aptitudes will be reported in due course.

Experimental

All organic solvents were anhydrous and of AR grade. Vacuum rotary evaporation was carried out at <30 °C. Analytical thin-layer chromatography was performed using Merck Kieselgel 60 F 254 silica plates; preparative column chromatography was performed on Merck 938S silica gel. Infra-red spectra were obtained using an FT/IR-4100 type A instrument. Both ^{1}H and ^{13}C NMR spectra were recorded for the solvents noted using either Bruker 250 MHz or 400 MHz instruments (the latter operating at 100 MHz for ^{13}C

observation) with tetramethylsilane as internal standard. Mass spectra in the chemical ionisation (CI) mode were obtained using a VG7070E mass spectrometer. Both low and high resolution electrospray mode (ES) mass spectra were obtained using a Micromass LCT mass spectrometer operating in the +ve or −ve ion mode as indicated. Elemental microanalysis was performed by Mr. Steve Apter (Liverpool). 3-[2,2,3,3–$^2H_4$] Trimethylsilyl propionate sodium salt (TSP), sodium dihydrogen phosphate and disodium hydrogen phosphate, were purchased from Sigma-Aldrich Company, Ltd (Gillingham, Dorset, UK). HPLC-NMR grade deuterium oxide (^2H_2O) was obtained from Goss Scientific Instruments (Essex, UK).

4-Methoxybenzyl-α,β-D-glucuronate 3

4-Methoxybenzyl bromide (0.94 mL, 5.67 mmol) was added to a solution of D-glucuronic acid (1 g, 5.15 mmol) and 1M TBAF in THF (5.41 mL, 5.15 mmol) in DMF (16 mL) which was stirred at 20 °C. Stirring was continued for 16 h, then the solution was evaporated to dryness and chromatographed, eluting with 20% ethanol–dichloromethane. Evaporation of appropriate fractions afforded the desired product **3** (1.15 g, 71%), which was recrystallised from dichloromethane–ether as a white solid. Found: C, 51.9; H, 5.6. $C_{14}H_{18}O_8 \cdot 0.5\ H_2O$ requires C, 52.0; H, 5.9%. HRMS, found, m/z, 337.0905; $C_{14}H_{20}O_8Na$ requires m/z, 337.0899; δ_H [$(CD_3)_2CO$]: For 1α-OH anomer, 3.35–3.45 (1 H, dd, 2-H) 3.65 (1 H, t, J = 9.0 Hz, 4-H), 3.73 (1 H, t, J = 8.9 Hz, 3-H), 3.82 (3H, s, CH_3O), 4.31 (1 H, J = 9.3 Hz, 5-H), 5.10–5.20 (2 H, ABqt, ArCH_2O), 5.17 (1 H, d, J = 3.1 Hz, 1-H), 6.95 and 7.36 (4 H, approx. dd, ArH); for 1β-OH anomer: 3.22 (1H, t, 2-H), 3.40 (1H, t, 3-H), 3.65 (1H, t, J = 9.0 Hz, 4-H), 3.82 (3H, s, CH_3O), 3.86 (1H, d, J = 9.8 Hz, 5-H), 4.57 (1H, d, J = 7.7 Hz, 1-H), 5.10–5.20 (2 H, ABqt, ArCH_2O), 6.95 and 7.36 (4H, approx dd, ArH); δ_C [$(CD_3)_2CO$, mixture of anomers] 56.0, 56.3, 67.2, 67.3, 73.2, 73.3, 73.6, 74.5, 76.2, 77.2, 94.3, 99.0, 115.1, 115.7, 129.3, 129.4, 131.1, 131.2, 136.1, 161.1, 162.7, 170.2 and 171.0; m/z (ES, +ve ion mode) 337 (MNa^+), 100%.

General procedure for the synthesis of benzyl or 4-methoxybenzyl 1-arylacetyl-β-D-glucopyranuronates 8, 10, 11 and 14

A mixture of the carboxylic acid **5**, **6** or **7** (0.6 mmol), benzyl **2**[33] or 4-methoxybenzyl D-glucuronate **3** (0.171 g, 0.6 mmol) and HATU (0.228 g, 0.6 mmol) was stirred in anhydrous acetonitrile (6 mL) with either NMM (0.22 mL, 0.202 g, 1.2 mmol) for **5** or DABCO (0.134 g, 1.2 mmol) for **6** and **7**. After optimum conversion as determined by TLC (10% EtOH–CH_2Cl_2), the reaction was quenched by addition of Amberlyst A-15 (H^+ form, 2 eq.) followed by brief stirring, filtration and evaporation. The crude product was purified by chromatography, eluting with 5% EtOH–CH_2Cl_2 to afford the product **8**, **10**, **11** or **14** as a foam with spectroscopic data as shown below.

4-Methoxybenzyl (1-phenyl)acetyl-β-D-glucopyranuronate 8

Yield 41%, white solid. Found: C, 60.35; H, 5.7; m/z, 455.1321. $C_{22}H_{24}O_9 \cdot 0.5\ H_2O$ requires C, 59.9; H, 5.7%; $C_{22}H_{24}O_9Na$ requires m/z, 455.1318; δ_H [$(CD_3)_2CO$] 3.32 (1 H, t, J = 8.5 Hz, 2-H), 3.43 (1 H, t, J = 9.0 Hz, 3-H), 3.54 (1 H, t, J = 9.3 Hz, 4-H), 3.60 (2 H, s, PhCH_2CO), 3.66 (3 H, s, CH_3O), 3.88 (1 H, d, J = 9.7 Hz, 5-H), 5.14 (2 H, AB qt, ArCH_2O), 5.59 (1 H, d, J = 8.1 Hz, 1-H), 6.77 and 7.20 (4 H, dd, ArH of PMB ester) and 7.10–7.20 (5 H, m, ArH of *Ph*CH_2); δ_C [$(CD_3)_2CO$] 41.5, 56.0, 67.6, 73.1, 73.9, 77.6 (x2), 96.0, 115.1, 128.2, 129.2, 129.6, 130.7, 131.2, 135.2, 161.1, 169.4 and 171.1; m/z (ES +ve mode) 455 (MNa^+, 100%).

Benzyl 1-[(α-methyl)phenyl]acetyl-β-D-glucopyranuronates 10 and 11

Combined yield, 0.162 g (65%).

Diasteroisomer 1. White foam (0.077 g). Found: m/z, 439.1362. $C_{22}H_{24}O_8Na$ requires m/z, 439.1369; δ_H [$(CD_3)_2CO$] 1.33 (3H, d, J = 7.2 Hz, CH_3CHAr), 3.28, 3.42 and 3.56 (3 H, 3 m, 2-H, 3-H and 4-H), 3.70 (1 H, q, J = 7.2 Hz, CH_3CHAr), 3.93 (1 H, d, J = 9.2 Hz, 5-H), 5.07 (2 H, s, PhCH_2O), 5.45 (1 H, d, J = 8.2 Hz, 1-H) and 7.07–7.30 (10 H, m, ArH); δ_C [$(CD_3)_2CO$] 19.5, 39.2, 46.4, 67.7, 73.1, 77.6, 77.7, 96.0, 128.3, 128.9, 129.2, 129.3, 129.7, 129.8, 137.3, 141.6, 169.5 and 174.0; m/z (ES, +ve ion mode) 439 (MNa^+), 100%.

Diasteroisomer 2. White foam (0.085 g). Found: m/z, 439.13680. $C_{22}H_{24}O_8Na$ requires m/z, 439.1369; δ_H [$(CD_3)_2CO$] 1.32 (3H, d, J = 7.2 Hz, CH_3CHAr), 3.30, 3.45 and 3.53 (3 H, 3 m, 2-H, 3-H and 4-H), 3.70 (1 H, q, J = 7.2 Hz, CH_3CHAr), 3.91 (1 H, d, J = 9.2 Hz, 5-H), 5.04 (2 H, s, PhCH_2O), 5.48 (1 H, d, J = 8.2 Hz, 1-H) and 7.07–7.30 (10 H, m, ArH); δ_C [$(CD_3)_2CO$] 19.7, 39.2, 46.4, 67.7, 73.1, 77.6, 77.7, 96.0, 128.3, 128.9, 129.2, 129.3, 129.7, 129.8, 137.3, 141.7, 169.3 and 173.9 and 206.6 (solvent signal); m/z (ES, +ve ion mode) 439 (MNa^+), 100%.

Benzyl 1-[(α,α-dimethyl)phenyl]acetyl-β-D-glucopyranuronate 14

White foam, yield 0.155 g (60%). Found: m/z, 453.1515. $C_{23}H_{26}O_8Na$ requires m/z, 453.1525; δ_H [$(CD_3)_2CO$] 1.55, 1.59 [6 H, 2 s, $(CH_3)_2$CAr], 3.40, 3.57 and 3.66 (3H, 3 m, 2-H, 3-H and 4-H), 4.07 (1H, d, J = 9.5 Hz, 5-H), 5.21 (2 H, s, PhCH_2O), 5.62 (1H, d, J = 8.1 Hz, 1-H) and 7.20–7.50 (10H, m, ArH); δ_C [$(CD_3)_2CO$] 27.1, 27.7, 47.9, 67.6, 73.0, 73.9, 77.6, 77.7, 96.2, 127.0, 127.9, 129.1, 129.3, 129.5, 129.7, 137.3, 145.8, 169.4 and 176.0; m/z (ES, +ve ion mode) 453 (MNa^+), 100%.

1-(Phenyl)acetyl-β-D-glucopyranuronic acid 9

The PMB ester **8** (91 mg, 0.21 mmol) was treated with a solution of 10% CF_3CO_2H in CH_2Cl_2 (0.91 mL) at 0 °C. After stirring for 3 h at 20 °C, the solvent was removed *in vacuo* and the residue was triturated with CH_2Cl_2, affording a solid which was filtered off, washed with further CH_2Cl_2 and dried to afford the desired product **9** (54 mg, 82%). The spectroscopic data of this compound were consistent with those previously described,[33] viz: δ_H [$(CD_3)_2CO$]: 3.32–3.38 (1H, t, 2-H), 3.43–3.50 (1H, t, 3-H), 3.52–3.59 (1H, t, 4-H) 3.61 (2H, s, CH_2), 3.86 (1H, d, J = 9.7 Hz, 5-H), 5.48 (1H, d, J = 8.0 Hz, 1-H) and 7.15–7.20 (5H, m, ArH); δ_C [$(CD_3)_2CO$]: 41.5, 72.9, 73.9, 77.1, 77.6, 95.9, 128.2, 129.6, 130.8,135.2, 170.4 and 171.2; *m/z* (ES –ve ion mode) 311 $[M - H]^-$ 100%.

General procedure for the deprotection of benzyl esters 10, 11 and 14[33]

A solution of the benzyl ester **10**, **11** or **14** (0.3 mmol) in ^{i}PrOH (5 mL) was stirred with 10% Pd–C (0.015 g, 10% w/w) under H_2 for 30 min. The catalyst was filtered off using Celite and the solid washed with further ^{i}PrOH, then the combined filtrate and washings were evaporated to dryness. Trituration of the crude product with ether afforded the desired product **12**, **13** or **15** as an amorphous white solid.

1-[(α-Methyl)phenyl]acetyl-β-D-glucopyranuronic acids 12 and 13

Diastereoisomer 1. Yield 0.095 g (97%). Found: C, 53.7; H, 5.9; m/z, 325.0939. $C_{15}H_{18}O_8 \cdot 0.5\ H_2O$ requires C, 53.7; H, 5.7%; $C_{15}H_{17}O_8(M - H)^-$ requires m/z, 325.0923; $\nu_{max.}(cm^{-1})$ 3700–3200 (br, s), 1736 (s), 1495 (w) and 1053 (vs); δ_H [$(CD_3)_2CO$]1.49 (3H, d, J = 7 Hz, CH_3CHAr), 3.42, 3.57 and 3.67 (3H, 3 m, 2-H, 3-H and 4-H), 3.86 (1H, q, J = 7 Hz, CH_3CHAr), 4.05 (1H, d, J = 9.2 Hz, 5-H), 5.60 (1H, d, J = 8 Hz, 1-H), 7.25–7.30 (1H, m, ArH) and 7.30–7.40 (4H, m, ArH); δ_C [$(CD_3)_2CO$]18.3, 45.0, 71.7, 72.5, 75.9, 76.3, 94.6, 127.0, 127.6, 128.5, 140.3, 169.1 and 172.7; m/z (ES, –ve ion mode) 325 $(M - H)^-$, 100% and 673 $[2 \times (M - H)^- + Na]$, 15%.

Diastereoisomer 2. Yield 0.090 g (92%). Found: C, 52.8; H, 5.7; m/z, 325.0913. $C_{15}H_{18}O_8 \cdot H_2O$ requires C, 52.3; H, 5.8%; $C_{15}H_{17}O_8(M - H)^-$ requires m/z, 325.0923; $\nu_{max.}(cm^{-1})$ 3700–3200 (br, s), 1736 (s), 1496 (w) and 1053 (vs); δ_H [$(CD_3)_2CO$] 1.48 (3H, d, J = 7 Hz, CH_3CHAr),3.44 (1H, m) and 3.55–3.70 (2H, m, 2-H, 3-H and 4-H), 3.86 (1H, q, J = 7 Hz, CH_3CHAr), 3.98 (1H, d, J = 9.2 Hz, 5-H), 5.61 (1H, d, J = 8 Hz, 1-H), 7.25–7.30 (1H, m, ArH) and 7.30–7.40 (4H, m, ArH); δ_C [$(CD_3)_2CO$] 18.5, 45.0, 71.6, 72.5, 75.9, 76.3, 94.6, 127.0, 127.6, 128.5, 140.4, 169.0 and 172.7; m/z (ES, –ve ion mode) 325 $(M - H)^-$, 100% and 673 $[2 \times (M - H)^- + Na]$, 8%.

1-[(α,α-Dimethyl)phenyl]acetyl-β-D-glucopyranuronic acid 15

Yield 0.090 g (88%). Found: C, 55.0; H, 6.2; m/z, 339.1077. $C_{16}H_{20}O_8 \cdot 0.5\ H_2O$ requires C, 55.0; H, 6.0%; $C_{16}H_{19}O_8$ $(M - H)^-$ requires m/z, 339.1080; $\nu_{max.}(cm^{-1})$ 3700–3200 (br,s), 1732 (s), 1500 (w) and 1070 (vs); δ_H [$(CD_3)_2CO$] 1.56, 1.60 [6H, 2 s, $(CH_3)_2C$], 3.40, 3.56 and 3.64 (3H, 3 m, 2-H, 3-H and 4-H), 4.00 (1H, d, J = 9.6 Hz, 5-H), 5.62 (1H, d, J = 8.0 Hz, 1-H), 7.23 (1H, m, ArH), 7.31 (2H, m, ArH) and 7.40 (2H, m, ArH); δ_C [$(CD_3)_2CO$] 25.8, 26.4, 46.6, 71.7, 72.5, 75.9, 76.4, 94.8, 125.8, 126.6, 128.3, 144.5, 169.0 and 174.8; m/z (ES, –ve ion mode) 339 $(M - H)^-$, 100%.

NMR spectroscopy, degradation rate measurements

^{1}H NMR spectroscopy was carried out at 310 K using a Bruker AVANCE600 NMR spectrometer at 600.13 MHz, with a broadband inverse (BBI) 5 mm probe. A standard water peak presaturation pulse sequence was used:[42] for further details of the pulse sequences, parameters and ^{13}C carbonyl carbon measurements, see ESI.‡

Computational methods

We adopted the approach of sampling the conformations of the molecules using a Monte Carlo molecular mechanics search, which includes a model for solvation by water, the results of which were then taken on to be optimised using DFT. The initial conformational searches for both ground and transition state structures for each AG were located using Spartan04 (http://www.wavefun.com/) using the MMFF94aq forcefield. In the case of the transition state a distance constraint from the nucleophilic alkoxide oxygen and carbonyl carbon of 2.27 Å was applied. Molecules were selected that had a Boltzmann distribution above 0.1. These initial geometries (typically ~7 ground state conformers and ~6 transition state conformers for each AG) were used as the starting point for the geometry optimization with no constraints at the DFT level of theory (B3LYP/6-31G**), using PC-GAMESS code[43] implemented on the University of Liverpool Linux cluster. This level of theory and basis set was found to predict stable stationary points on the potential energy surface while determining the influence of acyl group migration on the rate constant.[41] The importance of including diffuse functions in similar molecular systems has previously been reported,[44,45] and subsequent single point energy calculations were performed (B3LYP/6-31++G**) with solvent being accounted for using the PCM model.[46] The harmonic vibrational frequency calculations at B3LYP/6-31G** level were carried out to characterize all stationary points as minima or as first order (transition state). All calculations were carried out on the dianionic form of AG and singlet multiplicity. Thermodynamic energies were calculated using the rigid rotor and ideal gas approximations at 310 K. Scheme 1 demonstrates the two diastereomeric transition states obtained owing to the different orientation of the C=O of the AG. Atomic charges were calculated using Natural Bond Orbital analysis package (http://www.chem.wisc.edu/~nbo5/). Electronegativity (χ), hardness (η) and softness (S) are defined as follows:[47,48] Electronegativity $(\chi) = (E_{LUMO} + E_{HOMO})/2$, hardness $(\eta) = (E_{LUMO} - E_{HOMO})/2$, $S = 1/2\eta$. Fukui indices were defined as follows: $f^- = \sum(c_{HOMO.n})^2$ and $f^+ = \Sigma(c_{LUMO.n})^2$ where $c_{HOMO.n}$ are the coefficients of the atomic orbital X_n in the HOMO and $c_{LUMO.n}$ are the coefficients of the atomic orbital X_n in the LUMO.[48] These Fukui functions were normalised in order to be able to compare the reactivity of the different molecules.[47] Molecular structures were depicted using Molekel.[49] Surface area calculations were performed using Spartan04.

Acknowledgements

We are grateful to the BBSRC, EPSRC and AstraZeneca plc for funding (Ph.D. studentships to LI and CJ) and to Dr Ryan Bragg of AstraZeneca for valuable comments on the MS.

References

1 F. M. Kaspersen and C. A. A. Van Boeckel, *Xenobiotica*, 1987, **17**, 1451–71.
2 A. V. Stachulski and G. N. Jenkins, *Nat. Prod. Rep.*, 1998, **15**, 173–86.
3 W. F. Goebel, *J. Biol. Chem.*, 1938, **122**, 649–653.
4 R. B. Vanbreemen and C. C. Fenselau, *Drug Metab. Dispos.*, 1986, **14**, 197–201.
5 E. M. Faed, *Drug Metab. Rev.*, 1984, **15**, 1213–49.
6 H. Spahn-Langguth and L. Z. Benet, *Drug Metab. Rev.*, 1992, **24**, 5–48.

7 A. V. Stachulski, J. R. Harding, J. C. Lindon, J. L. Maggs, B. K. Park and I. D. Wilson, *J. Med. Chem.*, 2006, **49**, 6931–45.
8 J. R. Kenny, J. L. Maggs, X. Meng, D. Sinnott, S. E. Clarke, B. K. Park and A. V. Stachulski, *J. Med. Chem.*, 2004, **47**, 2816–25.
9 K. Akira, T. Uchijima and T. Hashimoto, *Chem. Res. Toxicol.*, 2002, **15**, 765–72.
10 N. Presle, F. Lapicque, S. Fournel-Gigleux, J. Magdalou and P. Netter, *Drug Metab. Dispos.*, 1996, **24**, 1050–7.
11 J. Wang, M. Davis, F. Li, F. Azam, J. Scatina and R. Talaat, *Chem. Res. Toxicol.*, 2004, **17**, 1206–1216.
12 H. Georges, N. Presle, T. Buronfosse, S. Fournel-Gigleux, P. Netter, J. Magdalou and F. Lapicque, *Chirality*, 2000, **12**, 53–62.
13 C. Volland, H. Sun, J. Dammeyer and L. Z. Benet, *Drug Metab. Dispos.*, 1991, **19**, 1080–1086.
14 S. J. Vanderhoeven, J. C. Lindon, J. Troke, G. E. Tranter, I. D. Wilson and J. K. Nicholson, *Xenobiotica*, 2004, **34**, 73–85.
15 P. C. Smith, J. Hasegawa, P. N. Langendijk and L. Z. Benet, *Drug Metab. Dispos.*, 1985, **13**, 110–112.
16 E. Skordi, I. D. Wilson, J. C. Lindon and J. K. Nicholson, *Xenobiotica*, 2005, **35**, 715–725.
17 R. W. Mortensen, U. G. Sidelmann, J. Tjornelund and S. H. Hansen, *Chirality*, 2002, **14**, 305–312.
18 C. H. Johnson, I. D. Wilson, J. R. Harding, A. V. Stachulski, L. Iddon, J. K. Nicholson and J. C. Lindon, *Anal. Chem.*, 2007, **79**, 8720–8727.
19 H. Hasegawa, K. Akira, Y. Shinohara, Y. Kasuya and T. Hashimoto, *Biol. Pharm. Bull.*, 2001, **24**, 852–855.
20 U. G. Sidelmann, S. H. Hansen, C. Gavaghan, H. A. J. Carless, J. C. Lindon, R. D. Farrant, I. D. Wilson and J. K. Nicholson, *Anal. Chem.*, 1996, **68**, 2564–2572.
21 G. Bradow, L. S. Kan and C. Fenselau, *Chem. Res. Toxicol.*, 1989, **2**, 316–324.
22 T. Ebner, G. Heinzel, A. Prox, K. Beschke and H. Wachsmuth, *Drug Metab. Dispos.*, 1999, **27**, 1143–1149.
23 P. C. Smith and J. H. Liu, *Xenobiotica*, 1993, **23**, 337–348.
24 H. Spahn-Langguth, M. Dahms and A. Hermening, *Adv. Exper. Med. Biol.*, 1996, **387**, 313–328.
25 R. W. Mortensen, O. Corcoran, C. Cornett, U. G. Sidelmann, J. C. Lindon, J. K. Nicholson and S. H. Hansen, *Drug Metab. Dispos.*, 2001, **29**, 375–380.
26 U. G. Sidelmann, A. W. Nicholls, P. E. Meadows, J. W. Gilbert, J. C. Lindon, I. D. Wilson and J. K. Nicholson, *J. Chromatogr., A*, 1996, **728**, 377–385.
27 S. J. Vanderhoeven, J. Troke, G. E. Tranter, I. D. Wilson, J. K. Nicholson and J. C. Lindon, *Xenobiotica*, 2004, **34**, 889–900.
28 S. J. Vanderhoeven, J. C. Lindon, J. Troke, J. K. Nicholson and I. D. Wilson, *J. Pharm. Biomed. Anal.*, 2006, **41**, 1002–1006.
29 J. Hasegawa, P. C. Smith and L. Z. Benet, *Drug Metab. Dispos.*, 1982, **10**, 469–473.
30 K. Akira, T. Taira, H. Hasegawa, C. Sakuma and Y. Shinohara, *Drug Metab. Dispos.*, 1998, **26**, 457–464.
31 A. W. Nicholls, K. Akira, J. C. Lindon, R. D. Farrant, I. D. Wilson, J. Harding, D. A. Killick and J. K. Nicholson, *Chem. Res. Toxicol.*, 1996, **9**, 1414–1424.
32 J. A. Perrie, J. R. Harding, D. W. Holt, A. Johnston, P. Meath and A. V. Stachulski, *Org. Lett.*, 2005, **7**, 2591–2594.
33 E. R. Bowkett, J. R. Harding, J. L. Maggs, B. K. Park, J. A. Perrie and A. V. Stachulski, *Tetrahedron*, 2007, **63**, 7596–7605.
34 F. H. C. Stewart, *Aust. J. Chem.*, 1968, **21**, 2543–2550.
35 P. G. M. Wuts and T. W. Greene, *Greene's Protective Groups in Organic Synthesis*, 4th ed.; Wiley-Interscience: 2007.
36 M. Shoji, T. Uno and Y. Hayashi, *Org. Lett.*, 2004, **6**, 4535–4538.
37 M. Tanaka, M. Okita and I. Yamatsu, *Carbohydr. Res.*, 1993, **241**, 81–88.
38 M. Warrier, L. S. Kaanumalle and V. Ramamurthy, *Can. J. Chem.*, 2003, **81**, 620–631.
39 G. A. Kraus and M. J. Taschner, *J. Org. Chem.*, 1980, **45**, 1175–1176.
40 H. Neuvonen, K. Neuvonen, A. Koch, E. Kleinpeter and P. Pasanen, *J. Org. Chem.*, 2002, **67**, 6995–7003.
41 E. A. Pritchina, N. P. Gritsan, G. T. Burdzinski and M. S. Platz, *J. Phys. Chem. A*, 2007, **111**, 10483–10489.
42 J. K. Nicholson, P. J. Foxall, M. Spraul, R. D. Farrant and J. C. Lindon, *Anal. Chem.*, 1995, **67**, 793–811.
43 A. A. Granovsky, PC GAMESS version 7.1, http://classic.chem.msu.su/gran/gamess/index.html.
44 J. H. Lii, B. Y. Ma and N. L. Allinger, *J. Computational Chem.*, 1999, **20**, 1593–1603.
45 M. Hoffmann and J. Rychlewski, *J. Am. Chem. Soc.*, 2001, **123**, 2308–2316.
46 R. Cammi and J. Tomasi, *J. Computational Chem.*, 1995, **16**, 1449–1458.
47 M. Karelson, V. S. Lobanov and A. R. Katritzky, *Chem. Rev.*, 1996, **96**, 1027–1043.
48 R. G. Parr and R. G. Pearson, *J. Am. Chem. Soc.*, 1983, **105**, 7512–7516.
49 P. Flükiger, H. P. Lüthi, S. Portmann and J. Weber, *MOLEKEL 4.0:* Swiss National Supercomputing Centre CSCS, Manno (Switzerland), 2000.